

# Perfusion abnormalities in mild cognitive impairment and mild dementia in Alzheimer's disease measured by pulsed arterial spin labeling MRI

Panagiotis Alexopoulos · Christian Sorg · Annette Förchler · Timo Grimmer · Maria Skokou · Afra Wohlschläger · Robert Perneckzy · Claus Zimmer · Alexander Kurz · Christine Preibisch

Received: 8 April 2011 / Accepted: 9 July 2011 / Published online: 24 July 2011  
© Springer-Verlag 2011

**Abstract** Alzheimer's disease (AD) and mild cognitive impairment (MCI), the transitional clinical stage between cognition in normal aging and dementia, have been linked to abnormalities in brain perfusion. Pulsed arterial spin labeling (PASL) is a magnetic resonance imaging (MRI) technique for evaluating brain perfusion. The present study aimed to determine regional perfusion abnormalities in 19 patients with mild dementia in AD and 24 patients with MCI as compared to 24 cognitively healthy elderly controls using PASL. In line with nuclear imaging methods, lower perfusion in patients with MCI and AD was found mainly in the parietal lobe, but also in angular and middle temporal areas as well as in the left middle occipital lobe and precuneus. Our data imply that PASL may be a valuable instrument for investigating perfusion changes in the transition from normal aging to dementia and indicate that it might become an alternative to nuclear imaging techniques in AD diagnostics.

**Keywords** Pulsed arterial spin labeling (PASL) · Cerebral blood flow (CBF) · Mild cognitive impairment · Alzheimer's disease

## Introduction

Alzheimer's disease (AD) is the most common cause of dementia [35]. It is a neurodegenerative disorder that is pathologically defined by the presence of extracellular deposits of  $\beta$ -amyloid peptides in senile plaques, intraneuronal inclusions of hyperphosphorylated tau protein in neurofibrillary tangles, astrocytosis and synaptic as well as neuronal loss. The transitional stage between cognition in normal aging and dementia is commonly referred to as mild cognitive impairment (MCI) and represents in many cases a prodromal phase of AD [51]. The pathological hallmarks of AD emerge in the areas of the brain that are involved in memory consolidation, especially in the medial temporal lobes [54]. At the early stages of the disease, synaptic and neuronal loss, which results in atrophy, is predominantly observed in the hippocampus [25, 41]. A significant elevation of  $\beta$ -secretase activity, being the key enzymatic player in the amyloidogenic processing of the amyloid precursor protein, has been observed predominately in the temporal lobes and to a lesser extent in the frontal lobes of patients with AD [19].

Modern imaging techniques are invaluable instruments in shedding light on the pathomechanisms of AD. Studies based on functional nuclear imaging methods have elucidated metabolic and perfusion decreases as well as amyloid depositions in parietal areas, lateral temporal areas, precuneus, posterior cingulate gyrus and the dorsolateral frontal cortex that becomes affected with disease

---

P. Alexopoulos (✉) · C. Sorg · T. Grimmer · R. Perneckzy · A. Kurz  
Department of Psychiatry and Psychotherapy,  
Klinikum rechts der Isar der TU München,  
Ismaninger Str. 22, 81675 München, Germany  
e-mail: panos.alexopoulos@lrz.tu-muenchen.de

C. Sorg · A. Förchler · A. Wohlschläger · C. Zimmer · C. Preibisch  
Department of Neuroradiology, Technische Universität München, Munich, Germany

M. Skokou  
Department of Psychiatry, University of Patras,  
Rion, Patras, Greece

C. Preibisch  
Department of Neurology, Technische Universität München, München, Germany

progression [15, 21, 24]. In recent years, MRI-based arterial spin labeling (ASL) techniques [7] have emerged as a scientific tool to investigate perfusion in patients with AD. Cerebral blood flow (CBF) effects the delivery of oxygen and nutrients to tissues and thus is correlated to brain functional activity and cerebral metabolic rate [8]. In ASL, perfusion contrast is obtained by manipulating the longitudinal magnetization of inflowing arterial blood water. The most consistent finding in ASL studies in patients with AD was a decreased CBF in precuneus and/or posterior cingulate cortex, as well as in lateral parietal cortex [4, 10]. Because of the limited spatial coverage and an increased vulnerability to artifacts, due to magnetic field variation, the findings of the few ASL studies, which investigated perfusion variations in medial temporal lobes in AD and MCI, are preliminary and remain controversial [4].

In light of the detected correlations between cerebral perfusion, assessed with nuclear imaging techniques, and pathological stage in AD [6], studying perfusion in the medial temporal lobes in patients with AD is crucial because of the paramount importance of this brain region in the development of AD pathology. Thus, the aim of the present study was to investigate regional CBF abnormalities mainly in the medial temporal and parietal lobes in patients with MCI and AD in comparison to elderly cognitively healthy controls [39] using a pulsed ASL technique (PASL) [20, 31]. We expected a reduction of CBF in both parietal and temporal lobes in patients with AD, since they are the brain regions, where AD pathology emerges [26, 35, 54].

## Methods

### Study sample

The study protocol was approved by the Ethics Committee of the Medical Faculty of the Technische Universität München. It was conducted in accordance with the 1964 Declaration of Helsinki. Written informed consent was available for all participants.

The participants were recruited at the Centre for cognitive disorders of the Department of Psychiatry and Psychotherapy and at the Department of Neuroradiology of the Technische Universität München. The diagnostic procedure included history from the patient and from an informant; medical, neurological and psychiatric examination, laboratory screening, structural brain imaging (MRI) and a neuropsychological examination based on the German version of the Consortium to Establish a Registry for AD neuropsychological assessment battery (CERAD-NAB) [47], which incorporates the mini-mental state examination (MMSE) [18].

The study sample embraced 24 cognitively healthy controls (HC) (8 male, 16 female, age  $67.1 \pm 6.1$  years), 24 patients with MCI (16 male, 8 female, age  $69.6 \pm 8.2$  years) and 19 patients diagnosed with mild dementia in AD (11 male, 8 female, age  $72.0 \pm 9.4$  years). Patients with AD fulfilled the criteria of the ICD-10 classification system for dementia [50] and the criteria of the National Institute of Neurological and Communicative Disorders and Stroke—Alzheimer's Disease and Related Disorders Association (NINCDS-ADRDA) for probable AD [34]. Patients with AD were treated with cholinesterase inhibitors and/or memantine. The diagnosis of MCI followed the revised consensus criteria of the International Working Group on MCI [51]. The HC were spouses and friends of the patients with clinically and neuropsychologically normal cognitive performance according to the MMSE. They were independent in their activities of daily living and did not have any memory complaints. HC candidates with serious medical, psychiatric or neurological disorders, which could affect cognitive functioning (e.g., major depression, posttraumatic stress disorder, stroke, schizophrenia, seizure disorder, head injury), with a score on MMSE  $<28$ , with structural MRI abnormalities potentially associated with cognitive deficits, or MRI contraindications were excluded from the study.

### Quantification of CBF

In the current study, the pulsed star labeling of arterial regions (PULSAR) technique was used [20] in combination with thin slice periodic saturation pulses (Q2TIPS) [31] applied between a first inversion time  $TI_1$  and the stop time  $TI_{1s}$ . This principally allows the calculation of quantitative CBF maps from data acquired with a single inversion time [31, 52]. For readout at the inversion time  $TI_2$ , a single-shot echo planar imaging [46] sequence was applied [32]. Calculation of quantitative perfusion maps from the difference signal  $\Delta S(\text{control-tag})$  was adapted from [38]. As there were no large arterial vessels in the tag and control images,  $S_{0B}$  was derived from WM signal ( $S_{WM}$ ), and CBF was calculated according to:

$$CBF = \frac{\Delta S(TI_2 + (n-1)ssTR)}{2 \cdot S_{0B} \cdot TI_1 \cdot \exp\left[-\frac{(TI_2 + (n-1)ssTR)}{T_{1B}}\right] \cdot \exp\left[-\frac{TE}{T_{2B}^*}\right]} \quad (1)$$

where  $n$  is the slice for which  $\Delta S$  is calculated,  $ssTR$  is the single slice repetition time,  $S_{0B}$  is the signal of fully relaxed blood,  $T_{1B}$  and  $T_{2B}^*$  are the longitudinal and effective transverse relaxation time of arterial blood, respectively. For quantitative calculation of CBF at 3.0 T,  $T_{1B}$  and  $T_{2B}^*$  were assumed to be 1.5 s and 100 ms [38].

## MR imaging protocol

MRI was performed on a 3-T whole-body MR scanner (Achieva, Philips Healthcare, Hamburg, Germany) using an 8-channel phased-array head coil (receive-only) and a whole-body transmit coil. Resting CBF maps were obtained from each participant. The acquisition parameters were as follows: TR/TE/ $\alpha$  = 2,500 ms/17 ms/90°;  $T_{1s}/T_{1s}/T_{1s}$  = 700 ms/1,200 ms/1,500 ms; 11 slices aligned to the hippocampus and comprising the parietal lobe were acquired from inferior to superior in an ascending order; acquisition time of a single slice ssTR = 42.2 ms; matrix size 64 × 63; voxel size 3.75 × 3.75 × 6 mm<sup>3</sup>; slice gap 0.6 mm; thickness of labeling slab 100 mm; distance between labeling slab and imaging volume 15 mm. Each perfusion measurement consisted of 80 pairs of label-control acquisitions with a scan time of 7 min and 18 s. To facilitate an accurate coregistration between perfusion and structural MRI data, a single-shot EPI volume covering the whole brain (voxel size 3.75 × 3.75 × 3 mm<sup>3</sup>; 40 slices) and a T1-weighted Turbo Field Echo [27] sequence (voxel size 1 × 1 × 1 mm<sup>3</sup>; 170 slices) were acquired in the same session. Each subject underwent routine clinical brain imaging with a FLAIR sequence to screen for existing brain disease. The participants were asked to rest and to keep their eyes closed during data acquisition.

## Data processing

Spatial preprocessing used SPM5 (<http://www.fil.ion.ucl.ac.uk/spm>) based on MATLAB and comprised motion correction, coregistration of perfusion-weighted images and anatomical T1-weighted images, segmentation, spatial normalization and smoothing (Gaussian kernel, 12 mm full width at half maximum). Since direct coregistration of the perfusion-weighted and T1-weighted MR images is not reliable, due to the low signal-to-noise ratio, the limited structural features and the low volume coverage of the perfusion-weighted images, a stepwise coregistration strategy was employed, similar to that described by Johnson et al. [30]. First, the T1-weighted structural image was coregistered using the whole brain EPI scan as a target. Subsequently, the whole brain EPI scan was coregistered using the mean image of the registered control and tag images as a target. The same transformations were then applied to the GM and WM segments of the structural scan. A binary WM mask was then created from the coregistered WM segment to determine  $S_{WM}$  and finally  $S_{OB}$ . Quantitative maps of CBF were then calculated according to Eq. 1. A correction of the perfusion data for partial volume effects (PVE) was performed according to the procedure described by Johnson et al. [30]. Partial volumes of GM

and WM are accounted for by the assumption that the perfusion to GM is 2.5 times greater than that to WM [44].

To facilitate normalization of CBF maps, a stepwise coregistration to anatomical data was performed. First, the mean of all tag and control images was registered to the whole brain EPI reference image, which then was registered to the T1-weighted image. The same transformations were then applied to the CBF map to achieve accurate coregistration to the structural T1-weighted image. Finally, the T1-weighted structural images were spatially normalized [5], and the same transformations were applied to the CBF maps. During this process, CBF maps got interpolated to a voxel size of 2 × 2 × 2 mm<sup>3</sup>. The normalized CBF maps were smoothed with an isotropic 12 mm full width at half-maximum Gaussian kernel to normalize the distribution of perfusion data as required within the framework of the subsequent statistical analyses and inference [53].

## Region of interest (ROI) analysis

Information on regional perfusion values was extracted by means of a region of interest (ROI) analysis. Anatomic ROIs were defined by means of the WFU Pickatlas tool ([http://www.nitrc.org/projects/wfu\\_pickatlas](http://www.nitrc.org/projects/wfu_pickatlas)). Global ROIs of GM were created by averaging the normalized GM segments (cognitively normal elderly subjects and the two patient groups separately), and applying a threshold of  $P_{GM} > 0.2$ . This corresponds to the area where voxel-wise partial volume correction (PVC) was applied. To restrict ROI evaluation to the measured volume, a mask was created from the normalized means of the registered control and tag images by averaging over subjects and applying appropriate thresholds. A custom program written in MATLAB was then used to calculate mean values of CBF within the masked anatomic ROIs for single subjects. Values within ROIs were then averaged for HC, patients with MCI and patients with AD.

## Voxel-wise analysis of variance (ANOVA)

CBF maps were statistically analyzed using second-level statistical procedures as implemented in SPM5 (<http://www.fil.ion.ucl.ac.uk/spm>). CBF differences between subject groups were explored by means of an ANOVA. Age and gender were used as covariates, since both have been shown to affect AD pathology [35, 40]. The following contrasts were performed: HC > MCI [1 −1 0], HC < MCI [−1 1 0], HC > AD [1 0 −1], HC < AD [−1 0 1], MCI > AD [0 1 −1], MCI < AD [0 −1 1]. The resulting parametric maps of  $t$  values were thresholded at  $P < 0.001$  uncorrected and at  $P < 0.05$ , corrected for multiple comparisons based on family-wise error (FWE) [37]. Anatomic

labeling of cluster localizations was aided by the automatic anatomic labeling toolbox [48].

## Results

### ROI analysis

Table 1 summarizes the results of the ROI analysis in global GM as well as in several anatomical ROIs. Even though the global mean of the partial volume corrected CBF ( $CBF_{corr}$ ) in GM in patients with MCI and AD was about 5 and 9% lower than in HC, these differences were not statistically significant. Compared to HC, patients with MCI and AD had statistically significant lower perfusion in the posterior cingulate gyrus and the lateral parietal lobe.  $CBF_{corr}$  was significantly higher in the middle temporal lobe and in the medial and lateral parietal lobe in HC in comparison to patients with AD. Higher perfusion in patients with MCI as compared to HC was observed in the

insula, rolandic operculum, putamen, Heschl's Gyrus, the superior temporal lobe/temporal pole, in the medial temporal lobe, in hippocampus and parahippocampus. However, statistical significance was only reached in the insula and putamen. No significantly elevated perfusion was observed in patient with AD compared with HC. The differences between the AD and MCI groups did not attain statistical significance according to the ROI analysis.

### Voxel-wise ANOVA

Figure 1 shows sections of T1-weighted anatomical images averaged over all HC with areas of lower  $CBF_{corr}$  in patients as revealed by the ANOVA analysis overlaid in yellow ( $P < 0.001$  uncorrected) and red ( $P < 0.05$ , FWE corrected). Table 2 summarizes anatomic regions, cluster sizes,  $z$  values and MNI coordinates of peak locations. Lower  $CBF_{corr}$  in patients with MCI as compared to HC was found in the right and left superior parietal gyrus, the right and left angular gyrus, the left inferior parietal gyrus,

**Table 1** Region of interest (ROI) analysis: cerebral blood flow with correction of partial volume effects ( $CBF_{corr}$ ) in a global gray matter (GM) ROI and in different anatomical GM ROIs for cognitively

healthy controls (HC), patients with mild cognitive impairment (MCI) and mild dementia in Alzheimer's disease (AD)

ROIs for CBF analysis	Actual ROI size (n voxel)	HC CBF (ml/100 g/min)	MCI CBF (ml/100 g/min)	AD CBF (ml/100 g/min)	<i>t</i> Test		
					HC > MCI $P \leq 0.05$	HC > AD $P \leq 0.05$	HC < MCI $P \leq 0.05$
Global CBF	71,113	41.8 ± 8.7	39.9 ± 9.5	38.0 ± 8.1	–	–	–
Frontal lobe							
Insula	3,355	39.1 ± 12.7	47.7 ± 13.7	46.5 ± 11.8	–	–	0.028
Rolandic operculum	2,195	53.0 ± 18.0	59.5 ± 14.8	57.0 ± 13.8	–	–	–
Deep GM							
Caudate	1,323	19.2 ± 5.8	17.3 ± 6.0	17.5 ± 7.6	–	–	–
Putamen	1,583	23.5 ± 5.1	27.6 ± 5.7	25.8 ± 7.0	–	–	0.012
Thalamus	1,450	44.6 ± 10.7	43.1 ± 18.3	40.2 ± 14.7	–	–	–
Temporal lobe							
Heschl	439	62.8 ± 20.6	70.7 ± 17.5	71.9 ± 14.5	–	–	–
Lateral temporal lobe							
Sup temp/temp pole	5,840	50.7 ± 11.5	54.1 ± 11.0	48.8 ± 10.3	–	–	–
Mid temp/temp pole	7,121	40.7 ± 9.6	35.4 ± 11.8	32.9 ± 11.3	–	0.020	–
Medial temporal lobe							
Hippocampus	1,190	35.8 ± 8.5	40.8 ± 11.6	37.7 ± 10.9	–	–	–
Parahippocampus	644	41.1 ± 11.7	46.7 ± 16.6	42.2 ± 8.4	–	–	–
Medial parietal lobe							
Precuneus	5,618	49.3 ± 12.2	41.2 ± 17.1	34.1 ± 12.2	–	0.0002	–
Post cingulate	522	50.3 ± 15.2	36.8 ± 18.6	32.3 ± 12.3	0.009	0.00009	–
Sup. lateral parietal	2,906	28.9 ± 10.1	16.0 ± 9.4	13.6 ± 7.6	0.00004	0.000001	–
Inf. lateral parietal	8,574	40.5 ± 10.2	32.5 ± 9.7	27.5 ± 9.0	0.008	0.00006	–
Inf. parietal	3,542	48.1 ± 14.1	32.3 ± 14.3	29.6 ± 10.7	0.0003	0.00001	–
Angular gyrus	2,681	44.7 ± 13.2	32.4 ± 14.2	26.7 ± 11.5	0.003	0.00002	–
Supramarginal gyrus	2,982	48.3 ± 12.7	47.8 ± 13.8	41.7 ± 12.4	–	–	–

**Table 2** Analysis of variance (ANOVA) (three groups, covariates age and sex): areas of hypo-perfusion in patients with mild cognitive impairment (MCI) and mild dementia in Alzheimer's disease (AD) compared with cognitively healthy controls (HC) at  $P < 0.001$  uncorrected, cluster size threshold 10

Anatomic location		Cluster Size	Voxel EquivZ	MNI coordinates		
				x	y	z
HC > MCI						
R	Sup. parietal	126	3.69	20	-64	66
R	Sup. parietal	24	3.2	34	-44	56
R	Angular*	370	4.46	46	-68	48
R	Mid. temporal	34	3.24	42	-68	14
L	Sup. parietal*	1,852	4.57	-26	-56	62
L	Inf. parietal		3.57	-44	-60	52
L	Inf. parietal	30	3.28	-44	-42	40
L	Angular	368	3.4	-36	-78	38
L	Mid. temporal		3.44	-40	-64	20
L	Mid. occipital		3.56	-32	-74	28
HC > AD						
R	Sup. parietal	25	3.25	22	-62	62
R	Inf. parietal	29	3.4	62	-38	50
R	Angular*	1,865	5	48	-66	48
R	Mid. occipital*		4.33	42	-72	18
L	Sup. parietal*	3,980	4.64	-34	-54	58
L	Inf. parietal		4.01	-30	-74	30
L	Precuneus*		4.33	-4	-64	48
L	Caudate	28	3.74	-14	-12	24
MCI > AD						
R	Mid. cingulate	17	3.44	8	-30	26

\*  $P < 0.05$  family-wise error (FWE) corrected

the left and right middle temporal gyrus and the middle occipital gyrus. Only the differences in the right angular gyrus and in the left superior parietal lobe survived FWE correction for multiple comparisons. Patients with AD showed lower  $CBF_{corr}$  than HC in the right angular gyrus, in the left and right superior parietal gyrus, in the left and right inferior parietal lobe, in the right middle occipital gyrus, in left precuneus and caudate. The differences in  $CBF_{corr}$  attained statistical significance on an FWE-corrected level in the left superior parietal lobe, in the right angular gyrus, in the middle occipital lobe and in the left precuneus. There was only a small cluster in the middle cingulate where patients with MCI exhibited higher perfusion than patients with AD. No regions of hyperfusion were detected in patients with AD and MCI compared with HC according to the ANOVA analysis.

## Discussion

The present study aimed to investigate regional CBF variations in medial temporal and parietal areas in patients with MCI and AD in comparison to HC using a PASL technique. Its main observations are focal areas of hypoperfusion in patients with AD and MCI as compared to HC mainly in the

parietal lobe, but also in middle occipital areas and in the middle temporal lobe. Moreover, the ROI analysis revealed significantly elevated perfusion in patients with MCI in the insular cortex as well as in putamen.

The finding of reduced perfusion in the precuneus, posterior cingulate gyrus, lateral parietal and middle occipital lobe is consistent with previous findings of ASL perfusion studies in patients with MCI and AD [4]. It is also concordant with a large amount of nuclear imaging data, showing severe hypometabolism, hypoperfusion and amyloid depositions in parietal regions in patients with MCI and AD [15, 21, 24]. Especially studies, which employed single photon emission computed tomography (SPECT) to assess perfusion, have shown that in patients with clinically diagnosed AD, hypoperfusion is robust in posterior cingulate cortex, precuneus and temporoparietal cortex [10]. Investigations with Fluorine 18-fluorodeoxyglucose positron emission tomography (FDG PET) revealed hypometabolism in parietotemporal associative areas and in posterior cingulate, where the retention of the  $^{11}C$  Pittsburgh compound B, a tracer binding to fibrillary  $\beta$ -amyloid, was found to be highest in mild AD [28, 35]. However, it is noteworthy that in our study, the CBF decreases that survived correction for multiple comparisons were mainly located in the parietal lobe, indicating that the

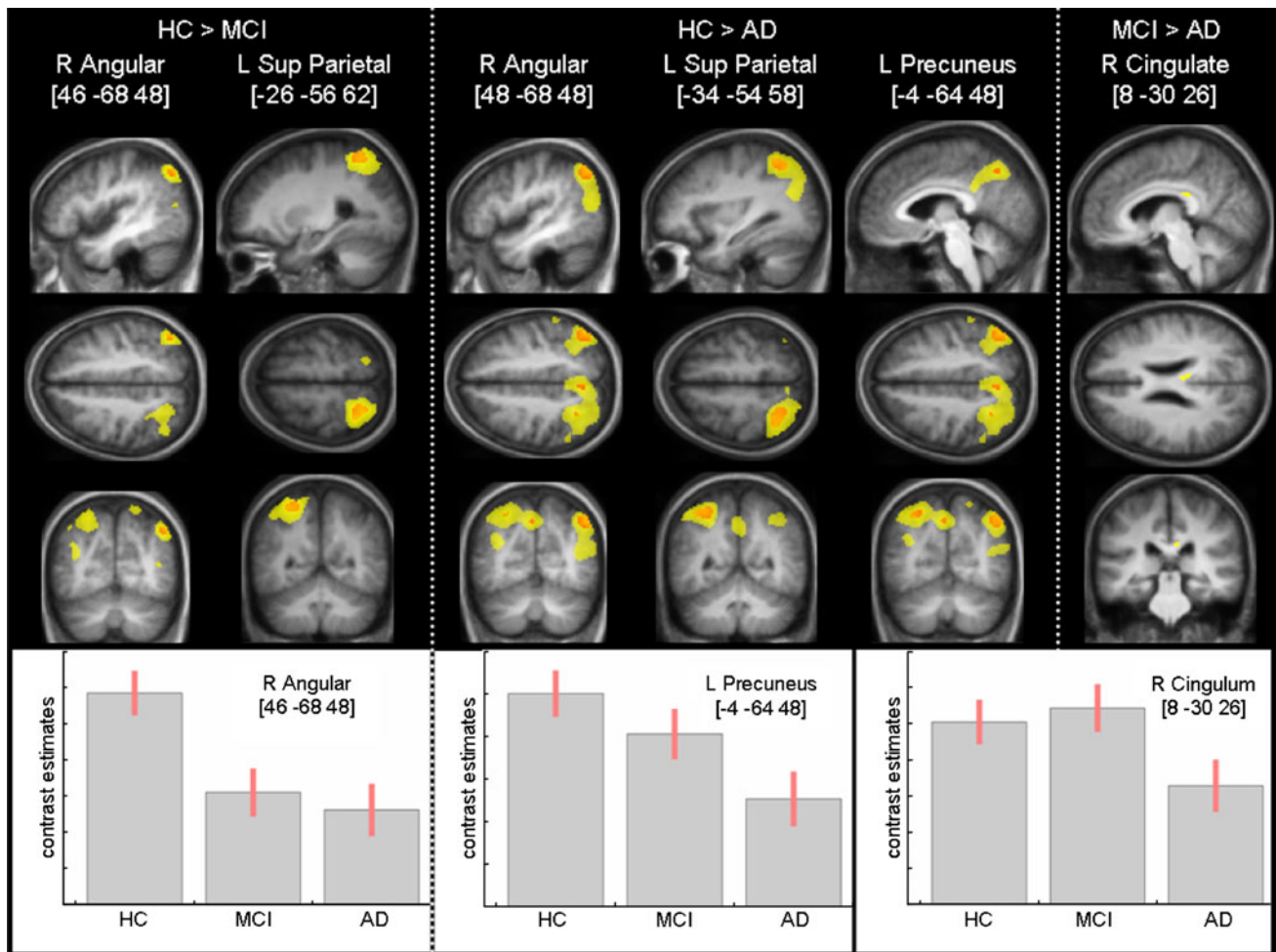


**Fig. 1** Analysis of variance (ANOVA) (three groups, covariates age and gender): areas of hypo-perfusion in patients with MCI and AD as compared with cognitively healthy controls (HC) (yellow:  $P < 0.001$  uncorrected; red:  $P < 0.05$  FWE corrected)

hypoperfusion observed in patients with AD and MCI reaches its zenith in this brain area. Reductions of CBF can be attributed to decreased activity per volume of GM or to reduced amounts of GM, as well as to synaptic loss and changes in neural activity owing to the progress of AD pathology (e.g., mitochondrial dysfunction and oxidative damage) [43]. In our study, PVE were taken into account. Thus, the detected CBF decreases in patients with MCI and AD are not merely a result of atrophy. Our findings are in line with an observed decrease in neural activity in parietal regions of patients with MCI and AD in memory-related functional MRI [9].

Though there is global agreement about the reduction of CBF, metabolic activity and amyloid deposition in parietal areas in patients with AD pathology, the effects of AD on temporal lobe seem to be more complex. In accordance with previous findings of ASL studies, we observed a CBF reduction in patients in the middle temporal lobe [13, 36]. Nevertheless, previous ASL studies that have taken into account PVE have detected an increase in perfusion in

parts of the medial temporal lobe, as well as in other regions (e.g., anterior cingulate, angular gyrus) [3, 12]. Although we did consider PVE, the ANOVA analysis did not show any areas of significant hyperperfusion in patients with AD and MCI. Interestingly, when global CBF of GM was considered as a covariate in the ANOVA analysis, we also obtained a significantly higher regional  $CBF_{corr}$  in patients with MCI than in HC in the medial temporal lobe, in occipital and frontal regions, while patients with AD exhibited higher  $CBF_{corr}$  in the insula, calcarine, temporal and frontal areas (data not shown). Even though these differences did not survive FWE correction for multiple comparisons, a correction for global CBF changes seems to facilitate the detection of hyperperfusion in patients with MCI and AD. Possibly, a similar effect occurred in the study of Alsop and colleagues [3] who performed a normalization of perfusion values to the visual cortex and detected significantly elevated CBF in the hippocampus and other medial temporal structures in patients with AD. Moreover, the ROI analysis of our data (Table 1) showed a

significantly elevated perfusion in the insular cortex and putamen as well as a trend to elevated perfusion in the superior and medial temporal lobe in patients with MCI compared with HC. It is noteworthy that the detected areas of statistically significant hyperfusion in patients with MCI in the ROI analysis are not located in brain regions that are affected by AD pathology [35]. The hyperfusion could be attributed to differences in gender distribution and age differences between the MCI and HC groups, which in contrast to the ANOVA analysis have not been taken into account in the ROI analysis. Differences in regional CBF patterns between genders, as well as the influence of age on perfusion and AD pathology, have already been described [22, 35, 45]. Nevertheless, it should be underscored that results of functional MRI studies indicate a hyper-activation of medial temporal lobe circuits early in the course of MCI before being comprised by AD pathology, whereas later in the course of MCI, as well as in mild AD, the medial temporal lobe was no longer capable to activate during attempted learning [14]. Moreover, SPECT studies revealed elevated CBF in rostral anterior cingulate in early stages of AD [29]. Hence, it cannot be ruled out with final certainty that the detected perfusion elevation in the ROI analysis may be a direct result of AD pathology, a response of neurons to the accumulation of neuritic plaques and neurofibrillary tangles, or a response to increased aberrant sprouting of cholinergic circuits. Alternatively, such increases may mirror a stage in the transition from normal cognition to dementia, which is marked by a neural compensatory response, being an attempt of the brain to compensate for the structural and functional lesions associated with the neurodegenerative process. This compensatory response may lead to dependence on higher energetic resources to maintain neural effectiveness. It occurs prior to some threshold of neuropathology beyond which such compensation is not possible [29]. Factors unrelated to AD pathology, such as release of nitric oxide, a potent vasodilator, which can occur during inflammation and in connection with NMDA receptor signaling and plastic remodeling, may also be implicated in perfusion elevation [3]. It is of note that metabolism and perfusion in the medial temporal lobe are usually not assessed with nuclear medicine methods because of lower normal values of metabolism/perfusion than in the neocortical association cortices and partial volume effects arising from the significant hippocampal atrophy, manifesting early in the disease course [24]. Nonetheless, a few PET studies, which were focused on this brain region, revealed a decrease in metabolism in medial temporal lobe [13, 36].

According to our observations, significant CBF differences between patients with MCI and AD were restricted to a small area of lower perfusion in the middle cingulate gyrus of patients with AD. This finding supports the

assumption that in our study sample, the clinical phenotype of MCI was mainly caused by AD pathology, which had not yet reached the severity to manifest clinically with the symptoms of dementia [2]. Previous ASL studies also reported minimal perfusion differences between patients with MCI and AD [12].

The results of ASL studies concerning the localization of regions of hypoperfusion, but also of brain areas with CBF elevation in patients with AD pathology in the stage of MCI or/and mild dementia, are heterogeneous [4]. This variability is likely to arise from differences in the employed ASL techniques, in imaging volumes and statistical analyses but also from the heterogeneity of AD neuropathology and/or individual variability of disease expression [10], as well as from group differences linked to recruitment or diagnosis biases. In addition, a considerable heterogeneity among patients with AD both clinically and with regard to functional imaging has been observed [49]. Furthermore, our findings indicate an asymmetry in perfusion abnormalities in patients with AD and MCI. Such laterality was previously observed in FDG PET studies in MCI and mild AD [16] and in amyloid depositions as assessed with <sup>11</sup>C Pittsburgh compound B PET [42].

The current study should be viewed in the light of several limitations. The imaging volume was relatively restricted and excluded large portions of the frontal and occipital lobes, as well as the cerebellum. This precludes meaningful comparison with previous studies demonstrating perfusion decreases in frontal areas. Moreover, it should be underlined that hypoperfusion cannot be attributed exclusively to AD pathology, due to the fact that other pathomechanisms such as age-related cerebrovascular alterations (e.g., ultrastructural changes in blood vessels, reduced vascular reactivity and tortuous cerebral vessels) [11, 23] may lead to an insufficient blood supply in the aging brain, resulting in reduction of CBF. In our study, participants were not checked for abnormalities of the blood vessels, supplying the brain. Even though there was no evidence of underlying neuropathology in our cognitively healthy subjects, an admixture of neurodegenerative changes influencing our results cannot be ruled out with final certainty. Furthermore, a generalization of our results should be treated with caution, since the study sample was relatively small. As a result, future studies are warranted to replicate our observations. A possible confounding effect of the treatment of patients with AD with cholinesterase inhibitors and/or memantine is rather unlikely, because the aforementioned treatment is symptomatic and does not affect the accumulated AD pathology in the brain. Finally, it should be underscored that clinical diagnoses based on international diagnostic criteria are not always confirmed at autopsy. Thus, a possible erroneous clinical assessment,

despite the comprehensive diagnostic work-up, should be taken into account [1].

In conclusion, ASL is a promising imaging technique in studying perfusion changes related to AD pathology. In light of our findings and taking into account its advantages over nuclear imaging methods (no exposure to ionizing radiation, no intravenous contrast agents or radioactive isotopes), it can be reckoned that ASL might become a part of AD diagnostics in the near future. Nonetheless, it is important to underscore the significant variability in the details of perfusion patterns in the early phase of AD, which possibly limits the clinical utility of ASL [33]. Further studies, combining nuclear imaging methods, measuring metabolism, perfusion and amyloid pathology, with ASL are warranted to investigate possible correlations/linkages between the localization and severity of the changes in metabolism, perfusion and amyloid deposition in patients with AD, in order to judge the clinical relevance of perfusion alterations [17] and unveil the pathomechanisms of a disease, which is assumed to become a global health scourge.

**Acknowledgments** We would like to thank all the healthy and diseased volunteers who participated in this study. AMW is supported by the German Federal Ministry of Education and Research, BMBF grant 01EV0710.

**Conflict of interest** None.

## References

- Alexopoulos P, Greim B, Nadler K, Martens U, Krecklow B, Domes G, Herpertz S, Kurz A (2006) Validation of the Addenbrooke's cognitive examination for detecting early Alzheimer's disease and mild vascular dementia in a German population. *Dement Geriatr Cogn Disord* 22:385–391
- Alexopoulos P, Grimmer T, Perneczky R, Domes G, Kurz A (2006) Progression to dementia in clinical subtypes of mild cognitive impairment. *Dement Geriatr Cogn Disord* 22:27–34
- Alsop DC, Casement M, de Bazelaire C, Fong T, Press DZ (2008) Hippocampal hyperperfusion in Alzheimer's disease. *Neuroimage* 42:1267–1274
- Alsop DC, Dai W, Grossman M, Detre JA (2010) Arterial spin labeling blood flow MRI: its role in the early characterization of Alzheimer's disease. *J Alzheimers Dis* 20:871–880
- Ashburner J, Friston KJ (1999) Nonlinear spatial normalization using basis functions. *Hum Brain Mapp* 7:254–266
- Bradley KM, O'Sullivan VT, Soper ND, Nagy Z, King EM, Smith AD, Shepstone BJ (2002) Cerebral perfusion SPET correlated with Braak pathological stage in Alzheimer's disease. *Brain* 125:1772–1781
- Buxton RB, Frank LR, Wong EC, Siewert B, Warach S, Edelman RR (1998) A general kinetic model for quantitative perfusion imaging with arterial spin labeling. *Magn Reson Med* 40:383–396
- Buxton RB, Uludag K, Dubowitz DJ, Liu TT (2004) Modeling the hemodynamic response to brain activation. *Neuroimage* 23(Suppl 1):S220–S233
- Celone KA, Calhoun VD, Dickerson BC, Atri A, Chua EF, Miller SL, DePeau K, Rentz DM, Selkoe DJ, Blacker D, Albert MS, Sperling RA (2006) Alterations in memory networks in mild cognitive impairment and Alzheimer's disease: an independent component analysis. *J Neurosci* 26:10222–10231
- Chen W, Song X, Beyea S, D'Arcy R, Zhang Y, Rockwood K (2010) Advances in perfusion magnetic resonance imaging in Alzheimer's disease. *Alzheimers Dement* 7(2):185–196
- D'Esposito M, Deouell LY, Gazzaley A (2003) Alterations in the BOLD fMRI signal with ageing and disease: a challenge for neuroimaging. *Nat Rev Neurosci* 4:863–872
- Dai W, Lopez OL, Carmichael OT, Becker JT, Kuller LH, Gach HM (2009) Mild cognitive impairment and alzheimer disease: patterns of altered cerebral blood flow at MR imaging. *Radiology* 250:856–866
- de Leon MJ, Convit A, Wolf OT, Tarshish CY, DeSanti S, Rusinek H, Tsui W, Kandil E, Scherer AJ, Roche A, Imossi A, Thorn E, Bobinski M, Caraos C, Lesbre P, Schlyer D, Poirier J, Reisberg B, Fowler J (2001) Prediction of cognitive decline in normal elderly subjects with 2-[(18F)fluoro-2-deoxy-D-glucose/positron-emission tomography (FDG/PET). *Proc Natl Acad Sci U S A* 98:10966–10971
- Dickerson BC, Sperling RA (2008) Functional abnormalities of the medial temporal lobe memory system in mild cognitive impairment and Alzheimer's disease: insights from functional MRI studies. *Neuropsychologia* 46:1624–1635
- Dougall NJ, Bruggink S, Ebmeier KP (2004) Systematic review of the diagnostic accuracy of 99mTc-HMPAO-SPECT in dementia. *Am J Geriatr Psychiatry* 12:554–570
- Drzezga A, Lautenschlager N, Siebner H, Riemenschneider M, Willoch F, Minoshima S, Schwaiger M, Kurz A (2003) Cerebral metabolic changes accompanying conversion of mild cognitive impairment into Alzheimer's disease: a PET follow-up study. *Eur J Nucl Med Mol Imaging* 30:1104–1113
- Falkai P, Moller HJ (2010) Understanding mental disorders from neuronal networks to glial cells and proteomics. *Eur Arch Psychiatry Clin Neurosci* 260:441–442
- Folstein MF, Folstein SE, McHugh PR (1975) Mini-mental state. A practical method for grading the cognitive state of patients for the clinician. *J Psychiatr Res* 12:189–198
- Fukumoto H, Cheung BS, Hyman BT, Irizarry MC (2002) Beta-secretase protein and activity are increased in the neocortex in Alzheimer disease. *Arch Neurol* 59:1381–1389
- Golay X, Petersen ET, Hui F (2005) Pulsed star labeling of arterial regions (PULSAR): a robust regional perfusion technique for high field imaging. *Magn Reson Med* 53:15–21
- Grimmer T, Drzezga A, Kurz A (2010) Visualization of amyloid with positron emission tomography. Useful improvement in the diagnosis of dementia? *Nervenarzt* 81:602–606
- Hanyu H, Shimizu S, Tanaka Y, Takasaki M, Koizumi K, Abe K (2004) Differences in regional cerebral blood flow patterns in male versus female patients with Alzheimer disease. *Ajnr* 25:1199–1204
- Heo S, Prakash RS, Voss MW, Erickson KI, Ouyang C, Sutton BP, Kramer AF (2010) Resting hippocampal blood flow, spatial memory and aging. *Brain Res* 1315:119–127
- Herholz K, Carter SF, Jones M (2007) Positron emission tomography imaging in dementia. *Br J Radiol* 80(Spec No 2):S160–S167
- Hyman BT, Van Hoesen GW, Damasio AR, Barnes CL (1984) Alzheimer's disease: cell-specific pathology isolates the hippocampal formation. *Science* 225:1168–1170
- Jack CR Jr, Petersen RC, Xu YC, O'Brien PC, Smith GE, Ivnik RJ, Boeve BF, Waring SC, Tangalos EG, Kokmen E (1999) Prediction of AD with MRI-based hippocampal volume in mild cognitive impairment. *Neurology* 52:1397–1403



27. Jarstfer BS, Rich NM, Hobson RW 2nd, Geer TM (1980) Smoking, lipids, and atherosclerosis. *Mil Med* 145:521–524
28. Johnson KA (2006) Amyloid imaging of Alzheimer's disease using Pittsburgh Compound B. *Curr Neurol Neurosci Rep* 6:496–503
29. Johnson KA, Moran EK, Becker JA, Blacker D, Fischman AJ, Albert MS (2007) Single photon emission computed tomography perfusion differences in mild cognitive impairment. *J Neurol Neurosurg Psychiatry* 78:240–247
30. Johnson NA, Jahng GH, Weiner MW, Miller BL, Chui HC, Jagust WJ, Gorno-Tempini ML, Schuff N (2005) Pattern of cerebral hypoperfusion in Alzheimer disease and mild cognitive impairment measured with arterial spin-labeling MR imaging: initial experience. *Radiology* 234:851–859
31. Luh WM, Wong EC, Bandettini PA, Hyde JS (1999) QUIPSS II with thin-slice T1I periodic saturation: a method for improving accuracy of quantitative perfusion imaging using pulsed arterial spin labeling. *Magn Reson Med* 41:1246–1254
32. Mansfield P (1984) Real-time echo-planar imaging by NMR. *Br Med Bull* 40:187–190
33. Martins-de-Souza D (2010) Is the word 'biomarker' being properly used by proteomics research in neuroscience? *Eur Arch Psychiatry Clin Neurosci* 260:561–562
34. McKhann G, Drachmann D, Folstein M, Katzmann R, Price D, Stadlan E (1984) Clinical diagnosis of Alzheimer's disease: report of the NINCDS-ADRDA work group under the auspices of Department of Health and Human Services Task Force on Alzheimer's Disease. *Neurology* 34:939–944
35. Minati L, Edginton T, Bruzzone MG, Giaccone G (2009) Current concepts in Alzheimer's disease: a multidisciplinary review. *Am J Alzheimers Dis Other Dement* 24:95–121
36. Mosconi L, Tsui WH, De Santi S, Li J, Rusinek H, Convit A, Li Y, Boppana M, de Leon MJ (2005) Reduced hippocampal metabolism in MCI and AD: automated FDG-PET image analysis. *Neurology* 64:1860–1867
37. Nichols T, Hayasaka S (2003) Controlling the familywise error rate in functional neuroimaging: a comparative review. *Stat Methods Med Res* 12:419–446
38. Nöth U, Meadows GE, Kotajima F, Deichmann R, Corfield DR, Turner R (2006) Cerebral vascular response to hypercapnia: determination with perfusion MRI at 1.5 and 3.0 Tesla using a pulsed arterial spin labeling technique. *J Magn Reson Imaging* 24:1229–1235
39. Pertoldi C, Hansen MM, Loeschcke V, Madsen AB, Jacobsen L, Baagoe H (2001) Genetic consequences of population decline in the European otter (*Lutra lutra*): an assessment of microsatellite DNA variation in Danish otters from 1883 to 1993. *Proc Biol Sci* 268:1775–1781
40. Placanica L, Zhu L, Li YM (2009) Gender- and age-dependent gamma-secretase activity in mouse brain and its implication in sporadic Alzheimer disease. *PLoS One* 4:e5088
41. Price JL, Davis PB, Morris JC, White DL (1991) The distribution of tangles, plaques and related immunohistochemical markers in healthy aging and Alzheimer's disease. *Neurobiol Aging* 12:295–312
42. Raji CA, Becker JT, Tsopelas ND, Price JC, Mathis CA, Saxton JA, Lopresti BJ, Hoge JA, Ziolko SK, DeKosky ST, Klunk WE (2008) Characterizing regional correlation, laterality and symmetry of amyloid deposition in mild cognitive impairment and Alzheimer's disease with Pittsburgh Compound B. *J Neurosci Methods* 172:277–282
43. Reddy PH, Beal MF (2008) Amyloid beta, mitochondrial dysfunction and synaptic damage: implications for cognitive decline in aging and Alzheimer's disease. *Trends Mol Med* 14:45–53
44. Roberts DA, Detre JA, Bolinger L, Insko EK, Leigh JS Jr (1994) Quantitative magnetic resonance imaging of human brain perfusion at 1.5 T using steady-state inversion of arterial water. *Proc Natl Acad Sci USA* 91:33–37
45. Rodriguez G, Warkentin S, Risberg J, Rosadini G (1988) Sex differences in regional cerebral blood flow. *J Cereb Blood Flow Metab* 8:783–789
46. Rosazza C, Minati L, Ghielmetti F, Maccagnano E, Erbetta A, Villani F, Epifani F, Spreafico R, Bruzzone MG (2009) Engagement of the medial temporal lobe in verbal and nonverbal memory: assessment with functional MR imaging in healthy subjects. *AJNR Am J Neuroradiol* 30:1134–1141
47. Thalman B, Monsch A (1997) The consortium to establish a registry for Alzheimer's disease. Neuropsychologische Testbatterie. *Memory Clinic Basel, Basel*
48. Tzourio-Mazoyer N, Landeau B, Papathanassiou D, Crivello F, Etard O, Delcroix N, Mazoyer B, Joliot M (2002) Automated anatomical labeling of activations in SPM using a macroscopic anatomical parcellation of the MNI MRI single-subject brain. *Neuroimage* 15:273–289
49. Warkentin S, Ohlsson M, Wollmer P, Edenbrandt L, Minthon L (2004) Regional cerebral blood flow in Alzheimer's disease: classification and analysis of heterogeneity. *Dement Geriatr Cogn Disord* 17:207–214
50. WHO (1994) Internationale Klassifikation psychischer Störungen, ICD-10 Kapitel V(F) Forschungskriterien. Hans Huber, Bern
51. Winblad B, Palmer K, Kivipelto M, Jelic V, Fratiglioni L, Wahlund LO, Nordberg A, Backman L, Albert M, Almkvist O, Arai H, Basun H, Blennow K, de Leon M, DeCarli C, Erkinjuntti T, Giacobini E, Graff C, Hardy J, Jack C, Jorm A, Ritchie K, van Duijn C, Visser P, Petersen RC (2004) Mild cognitive impairment—beyond controversies, towards a consensus: report of the International Working Group on Mild Cognitive Impairment. *J Intern Med* 256:240–246
52. Wong EC, Buxton RB, Frank LR (1998) Quantitative imaging of perfusion using a single subtraction (QUIPSS and QUIPSS II). *Magn Reson Med* 39:702–708
53. Worsley KJ (2003) Detecting activation in fMRI data. *Stat Methods Med Res* 12:401–418
54. Zetterberg H, Blennow K, Hanse E (2010) Amyloid beta and APP as biomarkers for Alzheimer's disease. *Exp Gerontol* 45:23–29